nature communications

Article

https://doi.org/10.1038/s41467-025-56352-5

A lightweight prosthetic hand with 19-DOF dexterity and human-level functions

Received: 29 November 2024

Accepted: 13 January 2025

Published online: 22 January 2025

Check for updates

Hao Yang[1,6], Zhe Tao[1,6], Jian Yang[2,6], Wenpeng Ma[1], Haoyu Zhang[1], Min Xu[1], Ming Wu[3], Shuaishuai Sun[1] ✉, Hu Jin[1] ✉, Weihua Li[4], Liu Wang[1,5] ✉ & Shiwu Zhang[1] ✉

A human hand has 23-degree-of-freedom (DOF) dexterity for managing activities of daily living (ADLs). Current prosthetic hands, primarily driven by motors or pneumatic actuators, fall short in replicating human-level functions, primarily due to limited DOF. Here, we develop a lightweight prosthetic hand that possesses biomimetic 19-DOF dexterity by integrating 38 shape-memory alloy (SMA) actuators to precisely control five fingers and the wrist. The prosthetic hand features real-time sensing of joint angles in each finger, feeding data into a control module for selectively heating or cooling SMA actuators in a closed-loop manner, mimicking the functioning of human muscles. Enabled by the high-power density of SMAs, the hand part (from the wrist to the fingertip) only weighs 0.22 kg, much lower than existing products. We also integrate an onboard power management module that provides electricity for operating the entire system. In addition to 33 standard grasping modes, this prosthetic hand supports 6 advanced grasping modes designed for enhanced dexterity evaluation, expanding the range of achievable ADLs for amputees while facilitating standard prosthesis function tests and validation in real-world scenarios. This innovation offers a significant advancement in prosthetic hand functions, promising improved quality of life for users.

Worldwide, approximately 11.3 million individuals with traumatic unilateral upper limb amputations face significant challenges in performing activities of daily living (ADLs)[1,2]. Wearable prosthetic hands are deemed the ultimate solution to recover lost hand functions. Despite the development over the past century, prosthetic hands are still facing a high abandonment rate of up to 39%[3] primarily due to the lack of comfort[4–6] and limited functions[7–9]. Without support from hand bones, the discomfort arises notably when prosthetic hands surpass the weight of a human hand (~400 g)[10,11], particularly evident in commercial products utilizing electric motors for finger control[12–18], such as those from Prensilia[12], Ossurs[13], and Ottobock[14,15] companies. To alleviate weight concerns, recent efforts have been devoted to developing prosthetic hands with pneumatically actuated soft fingers[19–21]. Representative advancements in prosthetic hands include the soft pneumatic models developed by Gu et al.[19] and Nemoto et al.[20], which weigh only 280 and 245 g, respectively.

However, compared with the 23-DOF dexterity of a human hand[22,23], existing prosthetic hands can typically offer no more than 10 DOFs, which is insufficient to replicate human-level functions for coordinated movements. For instance, the Feix GRASP taxonomy

[1]Institute of Humanoid Robots, School of Engineering Science, University of Science and Technology of China, Hefei 230026, China. [2]School of Electrical Engineering and Automation, Anhui University, Hefei, Anhui 230039, China. [3]The First Affiliated Hospital of USTC, Division of Life Sciences and Medicine, University of Science and Technology of China, Hefei, Anhui 230001, China. [4]School of Mechanical, Materials, Mechatronic and Biomedical Engineering, University of Wollongong, Wollongong, NSW 2522, Australia. [5]State Key Laboratory of Nonlinear Mechanics, Institute of Mechanics, Chinese Academy of Science, Beijing 100190, China. [6]These authors contributed equally: Hao Yang, Zhe Tao, Jian Yang. ✉e-mail: sssun@ustc.edu.cn; jhrdsp@ustc.edu.cn; wangliu05@ustc.edu.cn; swzhang@ustc.edu.cn

identifies 33 representative grasping modes of a human hand[24], of which 27 require more than 10 DOFs for precise execution (Supplementary Data 1). Due to the complexity of the human hand's 23 DOFs, this taxonomy only summarizes a portion of the human hand's grasping modes. The complexity is partially mitigated by the highly coupled proximal interphalangeal (PIP) and distal interphalangeal (DIP) joints in the index, middle, ring, and little fingers, suggesting that at least 19 DOFs are required to achieve dexterity comparable to that of human[25–27]. The low DOFs of existing prosthetic hands arise from the inherent challenge of the low power density, i.e., the power-to-weight ratio, of electric motors (100 W/kg) and pneumatic pumps (400 W/kg)[6]. Therefore, the tradeoff between human-comparable dexterity and minimal weight for comfortable wearing remains an unresolved conundrum in developing prosthetic hands.

Recent advancements in the field of robotics involve the application of shape-memory alloys (SMAs) actuators, known for their significant driving force, lightweight, and high deformability when electrically heated[28–31]. In contrast to electric motors and pneumatic pumps, SMAs exhibit a high-power density of 1000 W/kg[6], as shown in Supplementary Table 1. Leveraging this distinctive feature, SMAs have become prominent actuators in prosthetic hands[32–36]. For example, Bishay et al. utilized four pairs of SMA wires in a prosthetic hand, achieving a substantial pulling force of 70 N[34,36]. Due to the challenge of implementing closed-loop control for a large number of SMAs, their integration into prosthetic hands is still in the nascent stage, with existing prototypes yet to undergo validation on amputees due to issues such as bulky hardware and/or open-loop control algorithms[32–34] (see comparison in Supplementary Table 2).

Human-machine interaction is also crucial for prosthetic hands, and electromyography (EMG) technology has traditionally been used for intention recognition[37,38]. Pioneering neuroprosthetic hands such as those developed by Gu et al. (6 DOFs)[19], the Hannes hand (9 DOFs)[18], and the bebionic hand (6 DOFs)[14] have demonstrated the capabilities of EMG. However, while effective in systems with limited signal channels, it faces challenges in data acquisition and maintaining reliability and accuracy as the number of DOFs increases, notably up to 19 DOFs[39,40]. Other limitations may include frequent recalibration before use and performance degradation due to physiological factors such as sweating and muscle fatigue[1,41,42]. In contrast, voice command modules present a promising alternative for controlling high-DOF prosthetic hands, as detailed in Supplementary Data 2. These modules can achieve 95% recognition accuracy and offer millisecond-level response time[43]. Furthermore, voice command technology supports various languages, making it accessible and easy-to-learn to users worldwide, thereby offering a significant advantage for most amputees.

In this work, we report a lightweight, biomimetic prosthetic hand employing 19 pairs of highly integrated SMA actuators, enabling precise control of five fingers and the wrist, and achieving a remarkable 19-DOF dexterity (Fig. 1a and Supplementary Movie 1). The control mechanism involves a closed-loop system where voice recognition commands are translated to the SMA actuating system. The voice command technology, supported by iFLYTEK company—a global leader in voice recognition—offers a high accuracy of 95% and millisecond-level response times across 60 different languages. It incorporates voiceprint recognition technology and interfaces with a large language model, ensuring robust and personalized user interaction. Real-time sensing of joint angles, including bending and swing, facilitates selective heating or cooling of specific SMA actuators (Fig. 1b). The prosthetic hand is designed to closely mimic the human hand, comprising a hand part (from wrist to fingertip) and a forearm part (Fig. 1c). Capitalizing on the high-power density of SMAs, the total weight of prosthetic hand is 0.37 kg, and the hand part weighs only 0.22 kg while offering 19 DOFs, surpassing existing products and prototypes (see comparison in Fig. 1d and Supplementary Tables 2, 3). Our prosthetic hand can execute not only 33 standard grasping modes but also 6 more complex grasping modes, empowering amputees to seamlessly engage in various ADLs (Fig. 1e).

Results

Highly integrated prosthetic hand system

Figure 2a presents an overview of the prosthetic hand that is comprised of a hand part and a forearm part. A thin layer of silicone is molded on the hand part to mimic soft skin (Supplementary Fig. 1). The hand part mimics the human hand skeleton with 19 independent axes for bending, swinging, and rolling movements (Supplementary Movie 2)[44,45]. The forearm part houses several working modules including an actuating system with SMA springs and connecting cables, a control system with a drive circuit, a cooling fan, and a power management module with a lithium battery. The SMA actuators are arranged in the interlayer formed by the outer shell and inner lining of the forearm. Upon heating, SMA actuators transmit forces to a pulley mechanism via connecting cables to activate the movements of fingers and wrists. Each DOF is independently controlled by a pair of SMAs and a pair of cables. The drive circuit exercises selective control over the heating process of the SMA actuators. A cooling fan within the forearm enhances air circulation within the interlayer, facilitating rapid cooling of the SMA actuators. The lithium battery allows for the portable application of the prosthetic hand, which weighs totally 214 g (Supplementary Table 3). Considering that the average length of the right forearm is 25.4 cm in men and 23.5 cm in women[46], the forearm part length of the prosthetic hand is designed with a length of 23.3 cm, adjustable to a minimal length of 16 cm. The forearm's interior serves as a socket for amputees' residual limbs. Note that the maximum temperature during the 30-min continuous usage at the interior surface of the socket is 27.2 °C, which is safe for wearable application (Supplementary Fig. 2). A temperature management program has been integrated to halt the heating of SMAs immediately when the cooling fan stops, thereby enhancing patient safety. This highly integrated system emulates the intricate actuation mechanism of muscle, empowering the prosthetic hand to execute a diverse range of complex hand motions.

Biomimetic fingers/wrist with connecting cables

The human index, middle, ring, and little fingers have three joints, namely metacarpophalangeal (MCP), proximal interphalangeal (PIP), and distal interphalangeal (DIP) joints, from the palm to the fingertip (Fig. 2a). The MCP joint exhibits both bending and swing movements, while the PIP and DIP joints can bend only. Here, we choose the index finger as a representative finger to elucidate their analogous anatomical structures and corresponding connecting cables. For independent control of the bending and swing movements of the MCP joint, two pairs of cables are anchored to it, as depicted by the purple and red cables in Fig. 2b, respectively. Notably, the bending movement of the DIP joint is highly linked to the PIP joint[47,48], so a rod can be used to connect the PIP and DIP joints, leading to a four-bar linkage. As a result, a single pair of cables (depicted in green) suffices to achieve the coupled bending movement of the PIP/DIP joints (Fig. 2c). The kinematic analysis of the four-bar linkage mechanism is given in Supplementary Text 1 and Fig. 3. Detailed views of the swing/bending movement of the MCP joint and the bending movements of the PIP/DIP joint are presented in Fig. 2c.

The thumb exhibits a complex articulation involving three distinct joints: the carpometacarpal (CMC), MCP, and interphalangeal (IP) joints. The CMC joint demonstrates three DOF of bending, swing, and rolling movements. In contrast, the MCP and IP joints are characterized by bending motion only. Unlike the index finger, the thumb's IP joint has the unique capability to bend independently. Therefore, two pairs of cables are used to achieve independent control MCP and IP joint, as shown by the blue and green cables in Fig. 2d. For the CMC joint, three pairs of cables are employed to independently govern its bending,

swing, and rolling motions. Notably, the rolling motion of the human thumb's CMC joint, a passive DOF, allows for an average rotation angle of 17°[49], enhancing the thumb's ability to grasp objects smoothly and effectively. As depicted in the enlarged view in Fig. 2e, the CMC joint's rolling movement is specifically manipulated by a pair of red cables positioned on the palm.

In addition to five fingers, the human wrist can also have bending and swing movements. As shown in Fig. 2e, one end of the swing cables (depicted in purple) is affixed to the sides of the carpal bones and extends along the bending axis into the forearm. These cables facilitate the manipulation of the swing axis, thereby enabling the wrist to undergo swing motions within a range of ±12° (Fig. 2e, left). Simultaneously, one end of the bending cables (depicted in green) is connected to the cross shaft and extends into the forearm. These cables function to manipulate the bending axis, granting the wrist the capability to flex within a range of ±47° (Fig. 2e, right). Additionally, Supplementary Movie 3 illustrates the movements of the wrist of the prosthetic hand. The synergistic utilization of these cables allows for intricate control and coordination of the fingers and wrist, contributing to the versatile range of movements.

Comparative analysis of prosthetic hand dexterity

The prosthetic hand features 19 independent DOFs, with each joint's range of motion quantifiable by a specific angle. The angles of the

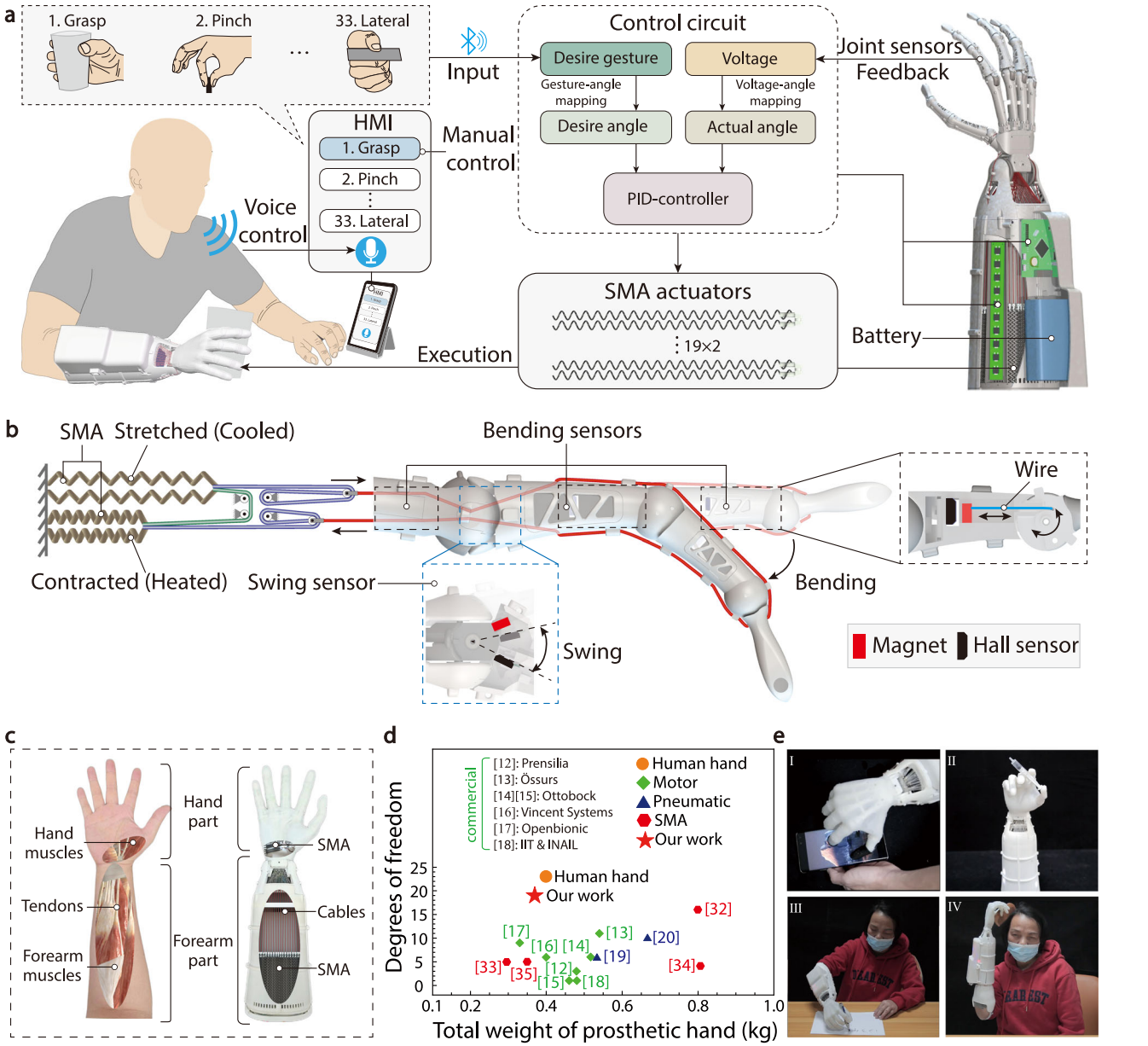

Fig. 1 | Overview of the lightweight prosthetic hand with 19-DOF dexterity and human-level functions. a Illustration of the working principles of the prosthetic hand: it interprets desired hand motions through a voice recognition module, processes commands via a control circuit, and executes motions by actuating 19 pairs of shape-memory alloy (SMA) actuators. **b** Schematic depiction elucidating the biomimetic finger structure, incorporating a dual SMA spring actuator for finger bending movements. Three customized bending sensors and one swing sensor utilizing hall sensors accurately detect the bending and swing angles of the finger joints. A spring actuator for the bending movement of the finger. **c** Comparison between our biomimetic prosthetic hand and the human hand. **d** Comparison between our prosthetic hand and existing works. Our prosthetic hand has 19 DOFs and the total weight is 370 g. **e** Practical demonstrations showcasing the prosthetic hand's dexterity in object manipulation and its capacity to restore human-level functions, such as writing and hair combing.

https://doi.org/10.1038/s41467-025-56352-5

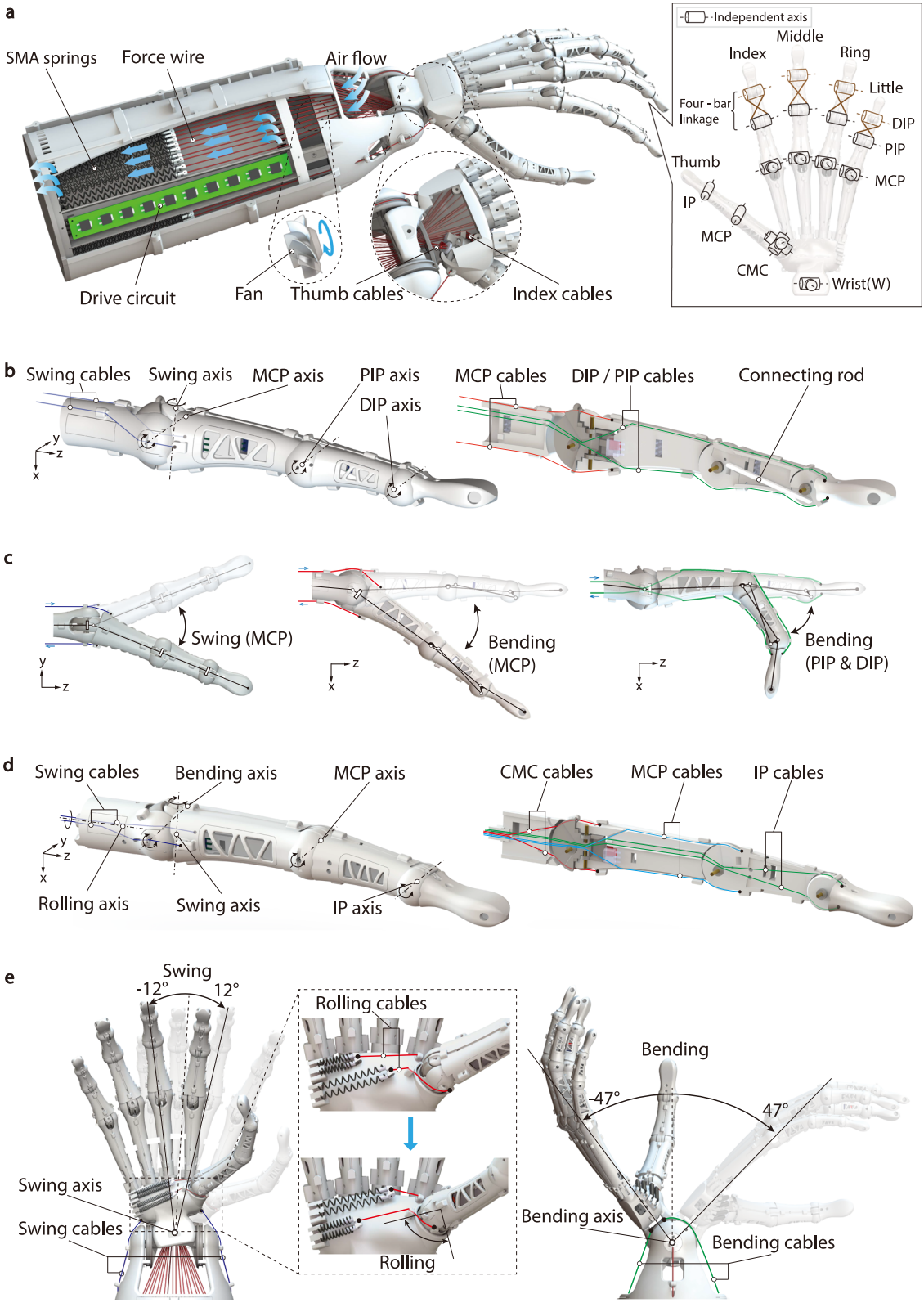

Fig. 2 | Biomimetic design of the highly integrated prosthetic hand. a Left: overview of the prosthetic hand in which 19 pairs of SMA springs actuate five fingers and wrist via 19 pairs of cables. The forearm part integrates SMA springs, cables, driving circuits, and a cooling fan. Right: 19 independent joint axes represent 19 DOFs of the prosthetic hand. MCP metacarpophalangeal, PIP proximal interphalangeal, DIP distal interphalangeal, CMC carpometacarpal, IP interphalangeal, SMA shape-memory alloy. **b** Left: overview of the index finger with swing cable actuating the swing movement of the MCP joint. Right: cross-sectional view showing cable connections to PIP and DIP joints. **c** Three joint movements of the index finger with corresponding cables. Left: swing movement of the MCP joint; Middle: bending movement of the MCP joint; Right: bending of the DIP and PIP joint via a four-bar linkage. **d** Left: overview of the thumb with swing cable actuating the swing movement of the CMC joint. Right: cross-sectional view showing cable connections to MCP and IP joints. **e** Left: swing of the wrist joint with a zoomed-in view of the rolling CMC joint of the thumb. Right: bending movement of the wrist.

https://doi.org/10.1038/s41467-025-56352-5

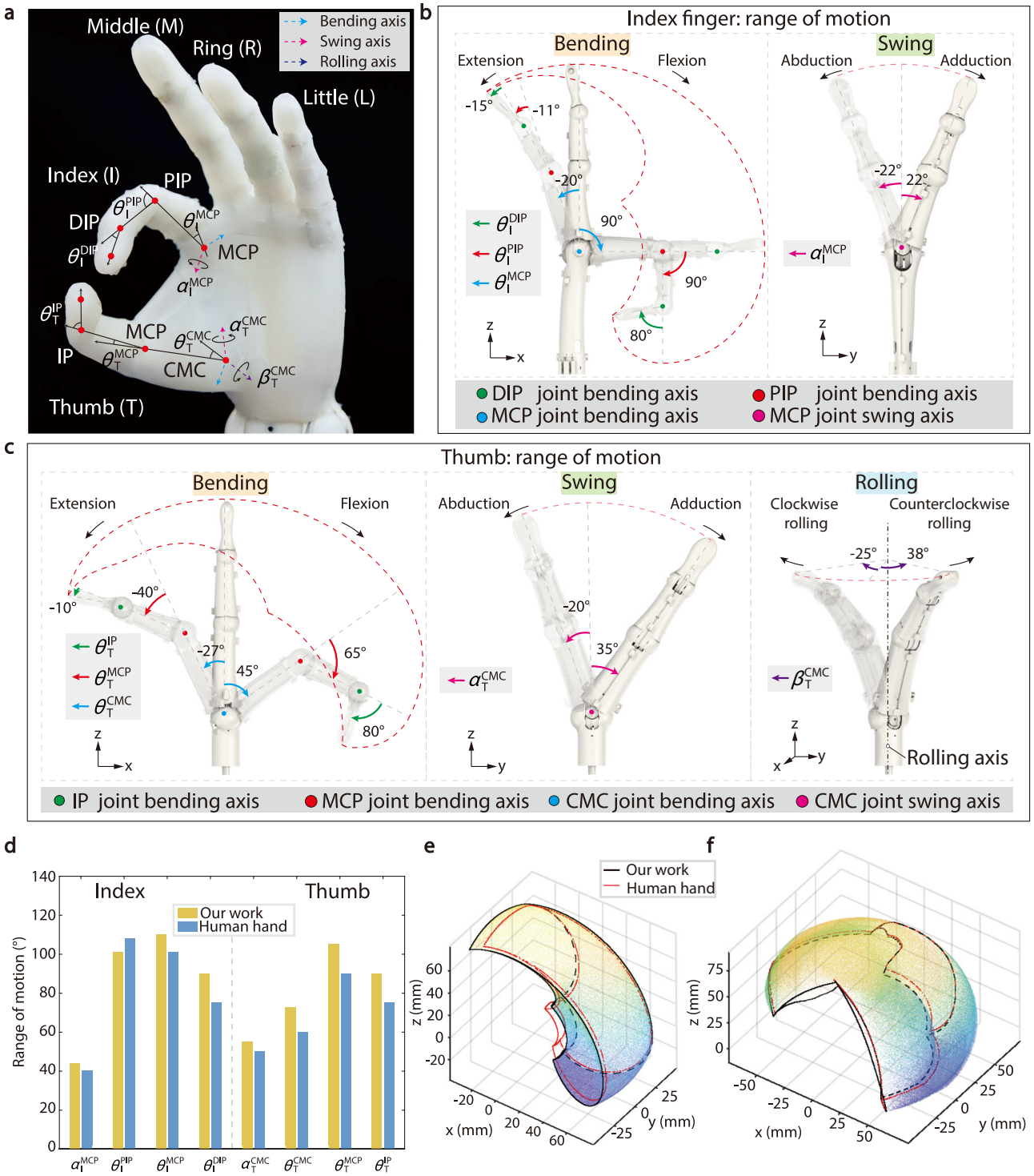

Fig. 3 | Comparative analysis of prosthetic hand dexterity. a Joint angles that quantify the dexterity of the index finger and thumb. MCP metacarpophalangeal, PIP proximal interphalangeal, DIP distal interphalangeal, CMC carpometacarpal, IP interphalangeal, θ bending, α swing, β rolling. **b** The range of motion of the index finger joints. **c** The range of motion of the thumb joints. **d** Comparative ranges of motion for the prosthetic hand's index and thumb joints versus those of a human hand. **e** Overlaid workspaces demonstrating the index finger's workspace for both the prosthetic and human hand. **f** Overlaid workspaces demonstrating the thumb's workspace for both the prosthetic and human hand.

index finger and thumb are labeled in Fig. 3a. The angles for bending, swinging, and rolling motions are represented by the symbols θ, α, β, respectively. Subscripts T, I, M, R, and L correspond to the thumb, index, middle, ring, and little fingers, while superscripts CMC, MCP, PIP, DIP, and IP denote the various joints. For instance, θ_I^{DIP} represents the bending angle of the DIP joint of the index finger. Figure 3b, c display the range of motion for the index finger and thumb, with dashed lines indicating the limits of fingertip position. We quantitatively compare the maximal joint angles—reflecting the range of motion—with those of the human hand in Fig. 3d. Evidently, the range of motion of our prosthetic hand is highly comparable to that of the human hand[23,40], with several joints having even larger angles. A

comparison of the range of motion of all joints is included in Supplementary Table 4. The large range of motion also yields a high workspace of the finger, i.e., the maximum reachable 3D space of the fingertip (Supplementary Text 2 and Fig. 4). The comparative diagrams in Fig. 3e, f, demarcated by black and red lines, illustrate the workspace for the prosthetic and human hands, respectively. This comparison assumes that both the human and prosthetic hands share identical joint structures and finger sizes. However, as noted in ref. 50, the human index finger's swing motion is constrained by lateral stiffness during bending, which limits its swing amplitude. In contrast, the MCP bending axis of the prosthetic hand's index finger is positioned below its MCP swing axis (Figs. 2b, 3b), allowing for constant swing amplitude across all bending angles. Therefore, the actual workspace of the human index finger is smaller as represented by the red line in Fig. 3e. Our data, further expounded upon in Supplementary Figs. 5, 6, indicate that the prosthetic hand's workspace not only emulates but also surpasses the natural range of motion of the human hand. Notably, the middle, ring, and little fingers show similar dexterity to the index finger.

Dual SMA actuation with closed-loop controllability

The prosthetic hand employs a dual SMA actuation system, analogous to the human hand's antagonistic muscle pair, enabling precise joint movements. The circuit system of the prosthetic hand is shown in Supplementary Fig. 7. Take the thumb as a representative finger since it has the most complicated motions. As shown in Fig. 4a, the flexion of the MCP joint is achieved by activating SMA2 to contract, while SMA1 is disengaged. Extension of the MCP joint is realized conversely, by heating SMA1 while cooling SMA2. This action is enhanced by a triple-force amplification mechanism (green lines). Note that the noise levels of the cooling fan in these operations are 61 dB, which are within acceptable ranges for daily activities, as shown in Supplementary Table 5. Additionally, the load capacity demonstration is detailed in Supplementary Table 6 and Supplementary Movie 4, showcasing fingertip force and grasping forces at different directions. The prosthetic hand can lift a payload of 2.5 kg and securely grasp a bottle of 1.3 kg. Considering that in nearly 10,000 grasping instances recorded by two housekeepers and two machinists, 92% of the objects weighed 500 g or less[51], the prosthetic hand is well-equipped to perform most tasks for daily use. The thumb's swing and rolling are similarly actuated (Fig. 4b, c). Sensing of joint angles are performed by Hall sensors paired with magnets attached to the joints via a thin yet stiff wire. When the joint moves, it pulls/pushes the magnet, translating magnetic field changes into voltage variations of the Hall sensor. It should be noted that calibration of the Hall sensor is essential prior to the initial use of the prosthetic hand, as shown in Supplementary Text 3 and Fig. 8. The calibration results indicate that the angle sensors can accurately reflect the five angles of the thumb, with an error lower than 0.5° (Fig. 4d). These readings allow for real-time monitoring and then are fed to the control circuit, which adjusts SMAs temperature via a widely used proportional–integral–derivative (PID) controller to match current postures with desired configurations. For example, precise control of each joint can be realized and demonstrated in Fig. 4e with a step response of the MCP bending θ_T^{MCP}, in Fig. 4f with a square response of the CMC swing α_T^{CMC}, and in Fig. 4g with a sine response of the CMC rolling β_T^{CMC}, respectively.

Through the integrated coordination of five pairs of SMA actuators, we can achieve closed-loop control over the finger's movements. For instance, Fig. 4h compared the actual angles of the thumb (solid lines) with the target values (dashed lines) during a power grasping gesture. The MCP joint of the thumb serves as a representative case, with its motion detailed in Fig. 4i. Before grasping, the target angles of each joint in the prosthetic hand are calibrated as shown in Supplementary Fig. 9. In the formal experiment, initially, at $t = 0$ s, $\theta_T^{MCP} = 20°$ with a 0% heating duty ratio. At $t = 1.5$ s, the palm opens to a preset angle of $\theta_T^{MCP} = -10°$, triggering the control module to heat SMA1 with a 100% heating duty ratio. As the MCP joint nears the target angle, the heating duty ratio decreases to 0% by $t = 2.6$ s. The subsequent command for power grasping sets $\theta_T^{MCP} = 5.4°$ at $t = 5.1$ s, prompting SMA2 to heat with a 100% heating duty ratio. When the desired angle is nearly reached at $t = 7$ s, the heating duty ratio is reduced to 0%, and the hand maintains a grasp. The average motion velocity of the finger joints is 63°/s, detailed in Supplementary Table 7. To assess the energy consumption and battery life of SMA prosthetic hands, simulations based on actual data were performed. As outlined in Supplementary Text 4 and Table 7, the battery capacity enables ~640 gestures according to the average energy consumption for a single grasping. Additionally, the SMA demonstrates high mechanical stability, enduring 10,000 cyclic stretching movements under a 7 N load, confirming its durability for prosthetic applications. This experimental data verifies that the SMA actuators, when empowered with positional feedback in a closed-loop system, facilitate stable and precise finger articulation, thus enhancing the prosthetic hand's functions.

Demonstration of prosthetic hand dexterity

The prosthetic hand's dexterity is methodically validated through a sequence of standard assessments as presented in Fig. 5. These evaluations incorporate standard Feix GRASP taxonomy (Fig. 5a and Supplementary Movie 5), Kapandji test[52] (Fig. 5b and Supplementary Movie 6), and additional hand gestures (Fig. 5C and Supplementary Movie 7). The Feix GRASP taxonomy classifies 33 standard grasping modes, which our prosthetic hand proficiently executes, as shown in Fig. 5a. Unlike traditional prosthetic hands, ours closely mimics the dexterity of a human hand, incorporating all swing DOFs, including adduction (clockwise swing) and abduction (anticlockwise swing). This addition significantly enhances the hand's workspace and grasping flexibility, prompting us to introduce 6 new daily grasping modes that fully utilize these swing DOFs (Supplementary Movie 8). These 6 new modes, depicted as Modes 34–39 in Fig. 5a, showcase advanced dexterity surpassing the standard Feix taxonomy (see in Supplementary Data 1). Modes 34–36, which include "rope organization", "pressing an electric pen" and "opening a rubber band with three fingers," highlight the intricate coordination between the thumb, index, and middle fingers. For example, Mode 34, "rope organization" is a precision grasp that involves thumb abduction with the index finger serving as a pivotal virtual third finger. Mode 37, "hand with ping pong paddle" and Modes 38, "overlapping pinch" and Mode 39, "dual-tool grasp," explore dynamic finger movements like the "OK" grasp and complex force applications, requiring sophisticated inter-finger coordination. These modes—particularly Modes 38 and 39—exemplify the prosthetic hand's capacity to perform complex tasks that extend beyond current classifications, demonstrating an enhanced simulation of human hand functionality.

Furthermore, we demonstrate the capabilities of replicating human hand gestures, including the Kapandji test (Fig. 5c) and a series of gestures denoting numbers 1–10 within the Chinese sign language context (Fig. 5c). The prosthetic hand not only matches the human hand in performing these gestures but also maintains the independence of non-engaged fingers. Gesture 6 from Fig. 5c, which deviates from typical synergistic hand postures, underscores the human-level capability despite that the prosthetic has 4 fewer DOFs compared with human hand. The prosthetic hand can also perform some hand manipulation tasks, as shown in Supplementary Movie 9. For instance, the task "use a syringe" utilizes the new grasping Mode 38, showcasing the practical applications and significance of the 19-DOF design.

Restoring human-level hand functions via voice interaction

Our prosthetic hand features a voice command system as a means of human–machine interaction, enabling the amputee to operate the prosthetic hand by verbal instructions. The voice command module

https://doi.org/10.1038/s41467-025-56352-5

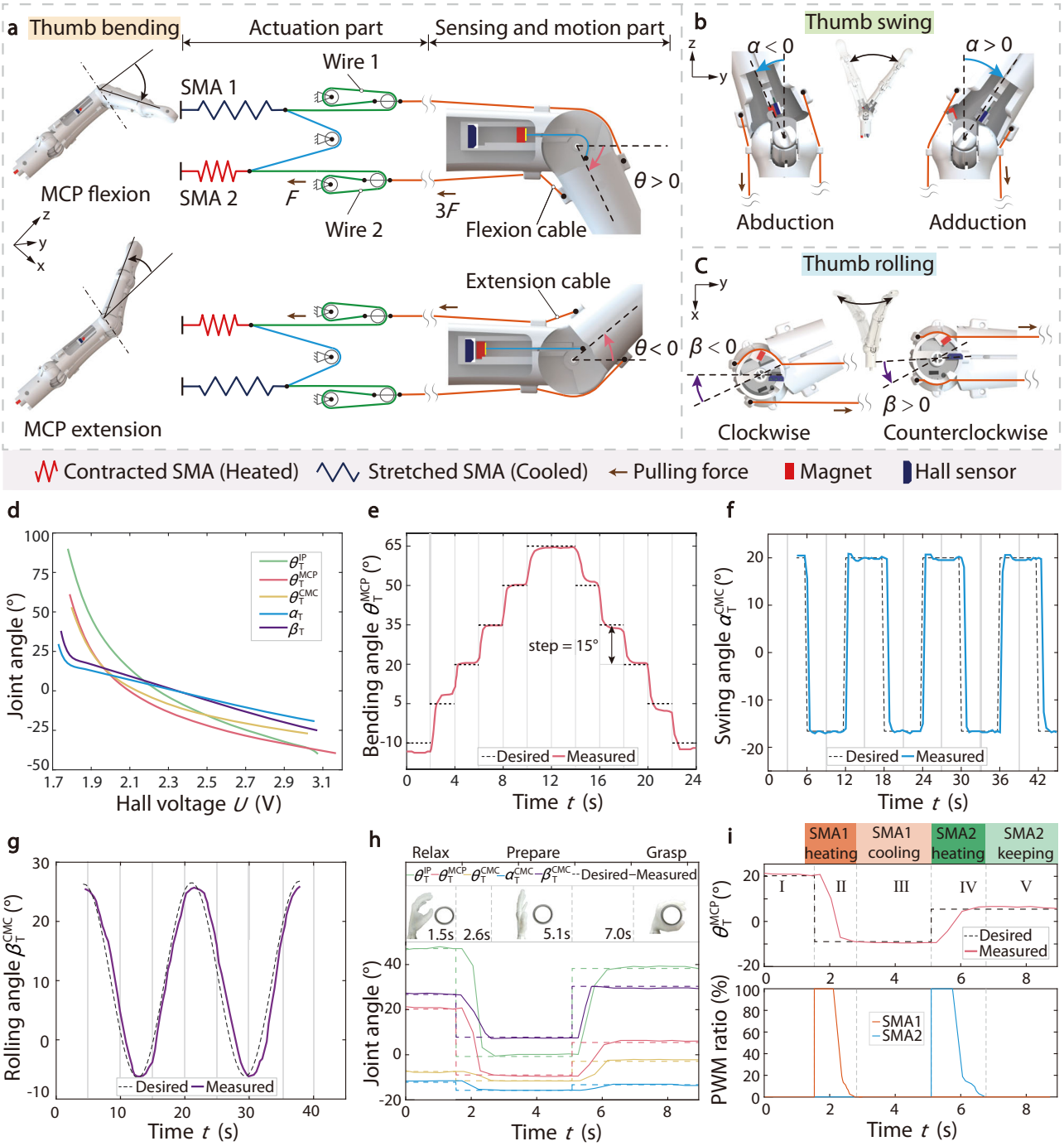

Fig. 4 | Dual SMA actuation with close-loop controllability. a Schematic diagram of the control system for the thumb MCP joint that includes SMA actuators, Hall sensors, and pulling cables. MCP metacarpophalangeal, SMA shape-memory alloy, θ bending, α swing, β rolling. **b** Quantification of thumb CMC swing. CMC carpometacarpal. **c** Quantification of thumb CMC rolling. **d** Calibration curve correlating Hall sensor voltage to joint angle. **e** Thumb MCP joint bending response to a step input. **f** Thumb CMC joint swing response to a square wave input. **g** Thumb CMC joint rolling response to a sine wave input. **h** Comparative analysis of actual and target joint angles during thumb grasping motions. IP interphalangeal. **i** The bending angle θ_T^{MCP} and heating duty ratio of SMA actuators under a step command.

we use, developed by iFLYTEK—a global leader in voice recognition technology—offers rapid recognition with millisecond-level response times and a high accuracy rate of 95%. Enhanced with voiceprint recognition, it accurately processes commands even in noisy environments (In a noisy home environment, where the noise reaches 60–70 dB, the accuracy of identifying four speakers is 97.42%[53]). This technology supports over 60 languages and 20 dialects, ensuring our prosthetic hand is accessible worldwide[43]. It is user-friendly, requiring no complex calibration, and its integration with advanced AI systems, like the iFLYTEK Large Language Model or ChatGPT, boosts its functionality.

A 60-year-old woman who had a right-hand amputation 1 year ago participated in our validation study. Without her dominant hand, she found daily tasks challenging to perform using only her non-dominant left hand. With minimal training of half a day on the voice control system, she was able to proficiently use the prosthetic hand,

Fig. 5 | Demonstration of prosthetic hand dexterity. a The GRASP taxonomy with all 33 standard and 6 new grasping modes. **b** The 8-score Kapandji test for validation of thumb dexterity. **c** Ten gestures denoting numbers 1–10 within the Chinese sign language context.

demonstrating the system's potential for quick adaptation and ease of use. The intuitive nature of the voice interaction system allowed for swift accommodation of the prosthetic hand, minimizing the need for preparatory adjustments prior to experimentation. These findings are documented in Fig. 6.

The results from standardized prosthetic function tests were promising. As shown in Fig. 6a and Supplementary Movie 10, the voice-controlled prosthetic hand performed proficiently in various tasks from Southampton Hand Assessment Procedure (SHAP)[54]. Here, we simply employ a non-amputee user to repeat the SHAP experiments for comparison of timing results, as shown in Supplementary Movie 11. With accurate recognition, the voice command module achieves a total response time of ~1.3 s from the initiation of speech to the activation of the SMA actuators. The prosthetic hand performed faster than the standard benchmark in four tasks but took a bit longer in seven other tasks (Supplementary Table 8). Despite these variances, the results suggest an avenue for increased efficiency through continued use and practice. Figure 6b and Supplementary Movie 12 show the hand's capabilities in tasks from the wolf motor function test (WMFT)[55], commonly used to evaluate hand function rehabilitation after a stroke. In Fig. 6c and Supplementary Movie 13, the prosthetic hand demonstrates its utility in four complex ADLs, such as combing hair, exchanging a business card and shaking a hand, writing with a three-finger pinch, and executing a chess capture. The voice commands used by the patient in the experiments are recognized and decoded, triggering the activation of corresponding SMAs to execute the specific task, as shown in Supplementary Table 9. These experiments utilized 11 different grasping modes across 22 patient trials, which account for nearly 90% of the total number of grasping modes used in daily life[56]. Both standard and six new grasping modes are demonstrated. For example, grasping mode 1-large diameter is conducted in experiments 5, 6, 12, and 20, while grasping mode 39-dual-

https://doi.org/10.1038/s41467-025-56352-5

Fig. 6 | Restoring human-level hand functions via voice command. a Evaluation of the prosthetic hand's capability through Southampton Hand Assessment Procedure (SHAP), involving 15 tasks that simulate daily activities: light and heavy spherical holds, light and heavy tripod grips, light and heavy power grips, light and heavy tip pinches, light extension, manipulating coins, opening a jar lid, pouring from a carton, handling an empty tin, carrying a tray, and turning a screw. **b** Further evaluation using the wolf motor function test (WMFT) includes three precise tasks: lifting a pen, stacking chess pieces, and flipping three pieces of paper. **c** Testing the prosthetic hand's grip and manipulation of commonly used items in activities of daily living (ADLs), exemplified by tasks such as combing hair, passing a business card and shaking a hand, writing with a three-finger pinch, and a chess capture.

tool grasp is conducted in experiment 22. These experiments highlighted complex interactions between the human and the prosthetic hand, presenting a rich variety of challenging scenarios. Remarkably, 20 out of 22 experiments were successful on the first attempt, indicating a 91% success rate. This high success rate underscores the prosthetic hand's enhanced stability and adaptability, facilitated by its extensive DOF. Moreover, the untested grasping modes are readily accessible and can be activated via voice commands by patients as needed in daily life.

It is also worth noting that, throughout the five-hour experiment, the patient reported no discomfort related to the prosthetic hand weight, performance, or voice control method. This confirms the device's suitability for extended use. The patient expressed increased confidence while wearing the prosthetic hand, noting it enabled performance comparable to other amputees and did not induce psychological pressure. Instead, it facilitated greater social participation. As the experiment progressed, a decrease in completion time for specific tasks was observed as the participant became more accustomed to the

prosthetic hand, manifesting the potential for enhanced functions and user adaptability.

To further demonstrate the stability of the prosthetic hand in daily life, we demonstrated picking fresh fruit using the prosthetic hand in a noisy outdoor market, as shown in Supplementary Movie 14. In an environment with a noise level ranging from 60 to 80 dB, the prosthetic hand successfully picked up various fruits, including jujubes, oranges, and grapes. Notably, no misrecognitions occurred in the voice command module during the process. Furthermore, the material cost of our prosthetic hand is approximately 3540 RMB, as detailed in Supplementary Table 10. This low-cost design significantly reduces the economic burden on patients, making it an accessible solution for people worldwide.

Discussion

Existing prosthetic hands, with DOFs far lower than a human hand (23 DOFs) cannot perform complex movements. To achieve a high DOF and low weight, we integrate 38 SMA actuators into a biomimetic prosthetic hand, which includes three major scientific contributions to the field of hand prosthetics. Firstly, the biomimetic design of structure and movements we proposed for the prosthetic hand incorporates a 19-DOF palm part (including fingers and wrist) and a forearm part, utilizing a muscle-like dual SMA actuation mechanism and the tendon-like transmission system. This strategy closely emulates the structural and kinematic characteristics of human hands by replicating the complex configurations of bones, muscles, and tendons. As a result, our developed prosthetic hand totally weighs only 370 g while offering 19 DOFs and 2.5 kg maximum load capability. Secondly, the closed-loop control mechanism of 19 DOFs ensures that the deformed states of each joint can be precisely sensed in real-time with 23 sets of Hall sensors, which enables closed-loop control of 19 DOFs for precise and coordinated hand movements (error smaller than 0.5°). This advanced control mechanism forms the foundation for executing various daily activities with high accuracy. Finally, the newly added grasping modes for dexterity evaluation introduced six new grasping modes that incorporate the adduction and abduction movements, in addition to the standard 33 grasping modes in Feix GRASP taxonomy. These new modes enhance the evaluation framework for prosthetic hand dexterity, providing a more comprehensive assessment of hand function.

EMG technology and voice command modules are both prevalent methods for human-computer interaction in prosthetic hands. We adopt the voice command module primarily for the following reasons. Firstly, the voice command module enables patients to quickly master the use of voice commands within just a few hours, without the complications associated with EMG technology such as dependence on wearing posture, movement of the prosthetic hand, and physiological factors like sweating and muscle fatigue. This usability is crucial for restoring independence in daily activities. Secondly, while EMG technology is widely used, it faces significant challenges in decoupling the 19 signals necessary for the independent control of 19 DOFs, often leading to unreliable operation. Additionally, EMG systems require frequent recalibration before each use, complicating their operation, especially for elderly users. Furthermore, the ability to control finger and wrist movements through voice commands allows users to achieve functionality close to that of a natural hand, greatly enhancing the quality of life for amputees. They can perform a wide array of tasks with increased confidence and precision. Lastly, integrating voice commands with a closed-loop control system that includes real-time angle sensing via Hall sensors ensures movements are precise and responsive. This level of control, difficult to achieve with EMG due to its susceptibility to signal variability, is crucial for tasks requiring continuous adjustment of grasp and finger positioning.

The basic performance parameters of our prosthetic hand—including weight, response time, joint movement speed, effectiveness of voice commands, load capacity, temperature management, energy consumption, battery life, durability, noise levels, and cost—have been thoroughly characterized. These detailed results substantiate the prosthetic hand's strong potential for practical application. Although the experiments primarily involved one patient in an indoor setting, the performance of the prosthetic hand was comprehensively demonstrated through these patient trials and additional testing.

The encouraging outcomes of our validation study demonstrate that this prosthetic hand has the potential to significantly alleviate the daily challenges faced by hand amputees, offering comfort, ease of use, and enhanced functional capacity. However, three primary limitations should be highlighted. Firstly, the absence of extensive clinical trials may potentially obscure certain issues that only emerge during real-world applications. Secondly, the effectiveness of the voice command module in daily scenarios may still be affected by background noise, speech impairments, or unrelated conversations from amputees themselves. Thirdly, latency remains a challenge in tasks requiring rapid hand movements.

Future research should prioritize long-term user trials in a wider patient demographic to collect further clinical data that evaluate the durability and practicality of the prosthetic hand across diverse real-world scenarios. Moreover, advancements in the voice command interface, combined with AI technology, could broaden the command spectrum, refine the control accuracy, and improve the response rate. The incorporation of tactile feedback would represent another significant step forward, providing users with essential sensory information and making the prosthetic hand feel even more like a natural limb.

Methods

Manufacturing of the prosthetic hand

In manufacturing the prosthetic hand, we employ an SLA 3D printer (Form 2, Formlabs) and Photopolymer resin (FLGPWH04, Formlabs) to manufacture the hand and forearm of the prosthetic hand. The prosthetic hand's five fingers, though varying in size, share a similar structure: each comprises four hinged sections, as depicted in Fig. 2b. Post assembly, we embed cables (PE braided line X9#0.6, CHUAZO) and Hall sensors (A1302KUA-T, Allegro MicroSystems) within the fingers. Subsequently, the fingers are attached to the carpal bone, through which the cables are threaded. This carpal bone connects via hinges to a cross shaft, and, subsequently, to the forearm. The forearm's interlayer houses the SMA springs (90 °C Flexinol actuator spring, DYNALLOY, Inc.) and the driving circuit. Lastly, the control circuit and the battery are mounted on the forearm's external shell, securely fastened by screws.

Manufacturing of the skin

3D CAD is utilized for designing both the skin model of the prosthetic hand and its corresponding casting molds. To simplify skin application, the model is segmented into six parts: five fingers and the palm, each with a dedicated mold. As illustrated in Supplementary Fig. 1, the left side features the casting mold for the palm skin, divided into five sections to simplify placement and positioning of the palm mold core, and assembled using screws. The casting mold for the finger skin, depicted on the right, is similarly assembled with screws. Silicone (Ecoflex 00-20, SMOOTH-ON, INC.) is then carefully poured into the molds and allowed to solidify. After the silicone setting, the skin is removed and fitted onto the prosthetic hand's skeletal structure. For a seamless appearance, the finger skins and palm skin are glued together, guaranteeing complete coverage over the hand part.

Sampling, control, and drive system

Supplementary Fig. 7 illustrates the circuit system of the prosthetic hand, comprising four functional modules: the sampling circuit and sensors, the drive circuit and SMA actuators, communications and controller, and power management. The sensor

module includes 23 Hall sensors, embedded within the hand's joints. Their signal lines converge at the ADC module (TLC1543, Texas Instruments) in the sampling circuit, which is serially connected to the MCU (STM32F103C8T6, STMicroelectronics). Within the sampling circuit, six electronic switches supply 3.3 V to the sensor groups. The MCU sequentially activates these switches, enabling the ADC module to read, digitize, and transmit the sensor groups' voltage signals via the serial peripheral interface to the MCU. The actuation module includes 38 units (ME60N03, Force-MOS Technology Co., Ltd) that heat SMA springs. Each unit comprises a signal receiver and a current output, the latter linked to the SMA spring, and the former to the PWM generator's (PCA9685, NXP Semiconductors) output, connected to the MCU through the I2C protocol. The MCU's signals control the PWM generator, thus regulating the actuator units' heating of the SMA springs. The Bluetooth serial module is split into two circuits: a voice collection circuit made up of the Bluetooth transceiver (HC-06, QinHeng Microelectronics) and the voice module, and a Bluetooth reception circuit combining the transceiver and the MCU. Both circuits engage in serial communication. The power management system's 12 V lithium battery (three cells, GREPOW) energizes the actuators. A step-down module (DM02-36050016DS, CDBARY) reduces the voltage from 12 to 5 V, and a voltage regulator (AMS1117, advanced monolithic systems) further lowers it to 3.3 V, supplying power to the MCU, Hall sensors, ADC module, PWM generator, and wireless communication module.

Image-based calibration system

As shown in Supplementary Fig. 8, four LED light (YLED0603YG, Shenzhen Yongyutai Electronics Co., Ltd.) sets are positioned along the lateral aspects of each thumb's four phalanges. The bending angles of the CMC, MCP, and IP joints is ascertained by measuring the angles between each set of LEDs. Furthermore, there are two sets of LED lights attached to the backside of the metacarpal bone and carpal bone, which are specifically used to measure the swing angle of the CMC joint. In addition, there are two sets of LED lights on the base and metacarpal bone, which are used together to measure the rolling angle of the CMC joint. All LED movements are captured at a 20 Hz frame rate using a camera (Mars5000S-35uc, Hangzhou Vision Datum Technology Co., Ltd.). The resulting images are then analyzed with MATLAB's Image Processing Toolbox to determine the bending, swing, and rolling angles of the thumb joints.

Performance characterization of the prosthetic hand

To evaluate repeatability, the SMA spring was tested under a 7 N load, corresponding to a stress of 34 MPa. Using a power supply (UTP1306S, Uni-Trend Technology Co., Ltd.), the spring was repeatedly heated and cooled for 10,000 cycles. During the process, its length varied between 10 and 18 centimeters. The change in length is recorded by a displacement sensor (OD1000-6001R15, SICK AG), and the number of cycles is recorded by a data acquisition circuit (STM32F103C8T6, STMicroelectronics). A force gauge (HANDPI™, SH-50) was used to measure the load capacity and fingertip force. A scale (EK813, Guangdong Senssun Weighing Apparatus Group Ltd.) was used to measure the weight of the bottle in Supplementary Movie 4. A decibel meter (GM1352, BENETECH™) was used to measure the noise level of the noise comparison experiment and the outdoor experiment.

Human–machine interface

Our human–machine interface incorporates the AI-powered voice recognition module AIUI Robot Multimodal Development Board (iFLYTEK Co., Ltd.) to facilitate voice-controlled interactions. The interface is programmed with three key functions: (1) Basic voice control commands like wake-up, gesture initiation, and stop, incorporating 35 actions based on the WMFT and SHAP experiments; (2) A status feedback feature reporting all of the joint angles and any anomalies of the prosthetic hand; (3) Manual control buttons, including multiple options for emergencies, such as an emergency stop. The voice recognition module we use is completely offline. The voice recognition process does not involve any data uploads; all voice inputs are directly processed and translated within the module. Consequently, there are no concerns regarding patient privacy leakage, nor can any monitoring behavior be implemented.

Human research participants

The recruited participant is a 60-year-old Chinese female who underwent right-hand amputation. Sex was determined based on self-report. The participant provided written informed consent for participation in all experiments and for the use of identifiable images in this work. Reasonable compensation was provided in the form of monetary compensation of 2000 RMB. Rehabilitation exercises on the individual are conducted by protocols approved by the Ethical Committee of the First Affiliated Hospital of the University of Science and Technology of China (number 2023KY060). Given the single-participant nature of this study, no sex or gender analysis was carried out.

Ethics

Every experiment involving animals, human participants, or clinical samples have been carried out following a protocol approved by an ethical commission. Each participant gave informed written consent.

Reporting summary

Further information on research design is available in the Nature Portfolio Reporting Summary linked to this article.

Data availability

All data supporting the findings of this study are available within the article and its supplementary files. Any additional requests for information can be directed to, and will be fulfilled by, the corresponding authors. Source data are provided with this paper.

Code availability

All the relevant codes are available at: https://github.com/Yanghao0506/A-lightweight-prosthetic-hand (ref. 57).

References

1. McDonald, C. L., Westcott-Mccoy, S., Weaver, M. R., Haagsma, J. & Kartin, D. Global prevalence of traumatic non-fatal limb amputation. *Prosthet. Ortho. Int.* **45**, 105–114 (2021).
2. Shahsavari, Hooman et al. Upper limb amputation; Care needs for reintegration to life: an integrative review. *Int. J. Orthop. Trauma Nurs.* **38**, 100773 (2020).
3. Smail, L. C., Neal, C., Wilkins, C. & Packham, T. L. Comfort and function remain key factors in upper limb prosthetic abandonment: findings of a scoping review. *Disabil. Rehabil.* **16**, 821–830 (2021).
4. Biddiss, E., Beaton, D. & Chau, T. Consumer design priorities for upper limb prosthetics. *Disabil. Rehabil.* **2**, 346–357 (2007).
5. Castellini, C. Upper limb active prosthetic systems—overview. *Wearable Robotics* 365–376 (2020).
6. Controzzi, M., Cipriani, C. & Carrozza, M. C. in *The Human Hand as an Inspiration for Robot Hand Development* (Balasubramanian, B. & Santos, V. J.) Ch. 11 (Springer, 2014).
7. Bicchi, A. Hands for dexterous manipulation and robust grasping: a difficult road toward simplicity. *Trans. Robot. Autom.* **16**, 652–662 (2000).
8. Brown, C. Y. & Asada, H. H. Inter-finger coordination and postural synergies in robot hands via mechanical implementation of

principal components analysis. *In Proc. 2007 IEEE/RSJ International Conference on Intelligent Robots and Systems* 2877–2882 (IEEE, 2007).
9. Bicchi, A., Gabiccini, M. & Santello, M. Modelling natural and artificial hands with synergies. *Phil. Trans. R. Soc. B.* **366**, 3153–3161 (2011).
10. Lewis, S., Russold, M., Dietl, H. & Kaniusas, E. Satisfaction of prosthesis users with electrical hand prostheses and their sugggested improvements. *Biomed. Eng. Biomed. Tech.* **58**, 000010151520134385 (2013).
11. Biddiss, E. A. & Chau, T. T. Upper limb prosthesis use and abandonment: a survey of the last 25 years. *Prosthet. Orthot. Int.* **31**, 236–257 (2007).
12. Prensilia. Mia hand. https://www.prensilia.com/wp-content/uploads/2023/03/Prensilia-robotics_data-sheet-Mia-Hand.pdf (2023).
13. Össurs. i-Limb. https://www.ossur.com/en-us/prosthetics/arms/i-limb-quantum (2023).
14. Ottobock. BeBionic Hand. https://www.ottobockus.com/prosthetics/upper-limb-prosthetics/solution-overview/bebionic-hand/ (2020).
15. Ottobock. MyoHand variplus speed. https://media.ottobock.com/_web-site/prosthetics/upper-limb/myoelectric_devices/files/prosthesis_systems_information_for_practitioners.pdf (2023).
16. Vincent Systems. Vincent hand. https://www.vincentsystems.de/en/vincent-evolution4 (2023).
17. O. B. labs. BRUNEL HAND 2.0. https://openbionicslabs.com/shop/brunel-hand (2022).
18. Laffranchi, M. et al. The Hannes hand prosthesis replicates the key biological properties of the human hand. *Sci. Robot.* **5**, eabb0467 (2020).
19. Gu, G. et al. A soft neuroprosthetic hand providing simultaneous myoelectric control and tactile feedback. *Nat. Biomed. Eng.* **7**, 589–598 (2023).
20. Nemoto, Y., Ogawa, K. & Yoshikawa, M. F3Hand II: a flexible five-fingered prosthetic hand using curved pneumatic artificial muscles. In *Proc. 2020 IEEE/SICE International Symposium on System Integration (SII)* 99–104 (IEEE, 2020).
21. Deimel, R. & Brock, O. A novel type of compliant and underactuated robotic hand for dexterous grasping. *Int. J Robot. Res.* **35**, 161–185 (2016).
22. Kapandji, I. A. The Physiology of the Joints, Volume I, Upper Limb. *Am. J. Phys. Med. Rehab.* **50**, 96 (1971).
23. Mallon, W. J., Brown, H. R. & Nunley, J. A. Digital ranges of motion: normal values in young adults. *J. Hand Surg.* **16**, 882–887 (1991).
24. Feix, T., Romero, J., Schmiedmayer, H.-B., Dollar, A. M. & Kragic, D. The grasp taxonomy of human grasp types. *IEEE Trans. Hum. Mach. Syst.* **46**, 66–77 (2015).
25. Santello, M., Flanders, M. & Soechting, J. F. Postural hand synergies for tool use. *J. Neurosci.* **18**, 10105–10115 (1998).
26. Thakur, P. H., Bastian, A. J. & Hsiao, S. S. Multidigit movement synergies of the human hand in an unconstrained haptic exploration task. *J. Neurosci.* **28**, 1271–1281 (2008).
27. Della Santina, C. et al. Postural hand synergies during environmental constraint exploitation. *Front. Neurorobotics* **11**, 41 (2017).
28. Zhakypov, Z., Mori, K., Hosoda, K. & Paik, J. Designing minimal and scalable insect-inspired multi-locomotion millirobots. *Nature* **571**, 381–386 (2019).
29. Koh, J.-S. et al. Jumping on water: surface tension–dominated jumping of water striders and robotic insects. *Science* **349**, 517–521 (2015).
30. Kim, D. et al. Actuating compact wearable augmented reality devices by multifunctional artificial muscle. *Nat. Commun.* **13**, 4155 (2022).
31. Sui, M. et al. A soft-packaged and portable rehabilitation glove capable of closed-loop fine motor skills. *Nat. Mach. Intell.* **5**, 1149–1160 (2023).
32. Cho, K.-J., Rosmarin, J. & Asada, H. SBC hand: a lightweight robotic hand with an SMA actuator array implementing C-segmentation. In *Proc. IEEE International Conference on Robotics and Automation (ICRA)* 921–926 (IEEE, 2007).
33. Deng, E. & Tadesse, Y. A soft 3D-printed robotic hand actuated by coiled SMA. *In Proc. Actuators* **10**, 6 (2020).
34. Bishay, P. et al. Design of a lightweight shape memory alloy stroke-amplification and locking system in a transradial prosthetic arm. *In Proc. Smart Mater. Adaptive Struct. Intell. Syst.* **85499**, V001T005A015 (2021).
35. Andrianesis, K. & Tzes, A. Development and control of a multi-functional prosthetic hand with shape memory alloy actuators. *J. Intell. Robot. Syst.* **78**, 257–289 (2015).
36. Bishay, P. L. et al. Development of a biomimetic transradial prosthetic arm with shape memory alloy muscle wires. *Eng. Res. Express* **2**, 035041 (2020).
37. Farina, D. et al. The extraction of neural information from the surface EMG for the control of upper-limb prostheses: emerging avenues and challenges. *IEEE Trans. Neural Syst. Rehabil. Eng.* **22**, 797–809 (2014).
38. Ciancio, A. L. et al. Control of prosthetic hands via the peripheral nervous system. *Front. Neurosci.* **10**, 116 (2016).
39. Zhuang, K. Z. et al. Shared human–robot proportional control of a dexterous myoelectric prosthesis. *Nat. Mach. Intell.* **1**, 400–411 (2019).
40. Moin, A. et al. A wearable biosensing system with in-sensor adaptive machine learning for hand gesture recognition. *Nat. Electron.* **4**, 54–63 (2021).
41. Ortiz-Catalan, M., Håkansson, B. & Brånemark, R. An osseointegrated human-machine gateway for long-term sensory feedback and motor control of artificial limbs. *Sci. Transl. Med.* **6**, 257re256–257re256 (2014).
42. Farina, D. et al. Toward higher-performance bionic limbs for wider clinical use. *Nat. Biomed. Eng.* **7**, 473–485 (2023).
43. iFLYTEK. https://www.xfyun.cn/services/voicedictation (2024).
44. Gustus, A., Stillfried, G., Visser, J., Jörntell, H. & van der Smagt, P. Human hand modelling: kinematics, dynamics, applications. *Biol. Cybern.* **106**, 741–755 (2012).
45. Emerson, E. T., Krizek, T. J. & Greenwald, D. P. Anatomy, physiology, and functional restoration of the thumb. *Ann. Plas. Surg.* **36**, 180–191 (1996).
46. Zarzycka, N. & Załuska, S. Measurements of the forearm i inhabitants of the Lublin region. *Ann. Univ. Mariae Curie Sklodowska. Med.* **44**, 85–92 (1989).
47. Kim, U. et al. Integrated linkage-driven dexterous anthropomorphic robotic hand. *Nat. Commun.* **12**, 1–13 (2021).
48. Roda-Sales, A., Sancho-Bru, J. L. & Vergara, M. Studying kinematic linkage of finger joints: estimation of kinematics of distal interphalangeal joints during manipulation. *PeerJ* **10**, e14051 (2022).
49. Cooney, W. P., Lucca, M. J., Chao, E. & Linscheid, R. The kinesiology of the thumb trapeziometacarpal joint. *J. Bone Joint Surg.* **63**, 1371–1381 (1981).
50. Zhou, P., Zhang, N. & Gu, G. A biomimetic soft-rigid hybrid finger with autonomous lateral stiffness enhancement. *Adv. Intell. Syst.* **4**, 2200170 (2022).
51. Feix, T., Bullock, I. M. & Dollar, A. M. Analysis of human grasping behavior: object characteristics and grasp type. *IEEE Trans. Haptics* **7**, 311–323 (2014).
52. Kapandji, A. Clinical test of apposition and counter-apposition of the thumb. *Ann. Chir. Main* **5**, 67–73 (1986).
53. Ma, F. et al. A spatial long-term iterative mask estimation approach for multi-channel speaker diarization and speech recognition. In *Proc.*

ICASSP 2024-2024 IEEE International Conference on Acoustics, Speech and Signal Processing (ICASSP) 12331–12335 (IEEE, 2024).
54. Burgerhof, J. G., Vasluian, E., Dijkstra, P. U., Bongers, R. M. & van der Sluis, C. K. The Southampton Hand Assessment Procedure revisited: a transparent linear scoring system, applied to data of experienced prosthetic users. *J. Hand. Ther.* **30**, 49–57 (2017).
55. Wolf, S. L. et al. Assessing wolf motor function test as outcome measure for research in patients after stroke. *Stroke* **32**, 1635–1639 (2001).
56. Kyberd, P. & Pons, J. L. A comparison of the oxford and manus intelligent hand prostheses. In *Proc. 2003 IEEE International Conference on Robotics and Automation (Cat. No. 03CH37422)* 3231–3236 (IEEE, 2003).
57. Yang, H. et al. A lightweight prosthetic hand with 19-DOF dexterity and human-level functions. *Zenodo* https://doi.org/10.5281/zenodo.14496961 (2024).

Acknowledgements

This work is funded by the National Natural Science Foundation of China under the following grant numbers: U21A20119 (awarded to S.Z.), 62473353 (awarded to H.J.), and 12272369 (awarded to L.W.). Additional support is provided by the Anhui Provincial Major Science and Technology Project (No. 202203a07020016, awarded to S.Z.). The authors appreciate C. Liu for agreeing to participate in this experiment; Y. Zhang and X. Zhang for their involvement in the design and construction of the experimental setup; and M. Sui and D. Wang for their discussions and suggestions on the paper content and illustrations.

Author contributions

H.Y., Z.T., and J.Y. contributed equally to this work. Conceptualization: H.Y., Z.T., H.J., L.W., and S.Z.; Methodology: H.Y., Z.T., J.Y., W.M. and H.Z.; Investigation: H.Y., Z.T., W.M., and H.Z.; Visualization: H.Y., Z.T., W.M., H.Z., L.W., and S.Z.; Funding acquisition: H.J., L.W., and S.Z.; Project administration: S.S., H.J., L.W., and S.Z.; Supervision: M.W., S.S., H.J., L.W., and S.Z.; Writing—original draft: H.Y., Z.T., J.Y., and L.W.; Writing—review and editing: H.Y., Z.T., M.X., S.S., H.J., W.L., L.W., and S.Z.

Competing interests

H.Y., M.X., H.J., and S.Z. are inventors of an invention disclosure of the patent filed by the University of Science and Technology of China (ZL201910524354.9, granted on 19 April 2022) related to structure design in this work. The remaining authors declare no competing interests.

Additional information

Supplementary information The online version contains supplementary material available at https://doi.org/10.1038/s41467-025-56352-5.

Correspondence and requests for materials should be addressed to Shuaishuai Sun, Hu Jin, Liu Wang or Shiwu Zhang.

Peer review information *Nature Communications* thanks Pedro Neto, and the other, anonymous, reviewer(s) for their contribution to the peer review of this work. A peer review file is available.